

Design and Performance of the Autonomous Data Acquisition System for the ARIANNA High Energy Neutrino Detector

Stuart A. Kleinfelder, *Senior Member, IEEE*, and The ARIANNA Collaboration

Abstract—The ARIANNA experiment will observe high-energy cosmogenic neutrino signatures via a large array of autonomous radio listening stations dispersed on the Ross Ice Shelf in Antarctica. Each station in the projected array of 900 stations will contain RF antennas, amplifiers, digitization, real-time triggering circuitry, a CPU with solid-state data storage, and redundant remote communications paths. Power is provided by both sun and wind. Two prototype stations have been installed, with a hexagonal array of seven stations, with each positioned 1 km apart, due for deployment over the next two seasons. The station's core data acquisition system includes four channels of analog sampling circuits that operate at 2 GHz and achieve over 11 bits of dynamic range. These circuits sample continuously over a 128-sample circular analog storage array. The circuits use a phase-locked loop to generate the 2 GHz internal sample clocking from a ~ 30 MHz external clock. Unlike most previous such designs, the high-speed sample clocking is completely synchronous and has very high timing stability, with about 1 ppm RMS jitter. The sampling circuits include the ability to produce a real-time trigger based on pattern-matching of the incoming waveform. Up to 72 patterns can be searched for in parallel, and each pattern looks at 8 consecutive samples, requiring that any or all of the samples be above a high threshold, below a separate low threshold, in-between the two thresholds, or a “don't care” condition. Each station also includes computing and solid-state event storage, environmental monitoring of voltage and power consumption, wind and temperature conditions, and both long-distance wireless to McMurdo Station and Iridium satellite communications. For the 2011–2012 austral season, about 1.4 million events were acquired between the second station's installation on December 21, 2011 and March 15, 2012.

Index Terms—Astrophysics experiment, data acquisition.

I. INTRODUCTION

THE ARIANNA experiment (Antarctic Ross Ice-shelf Antenna Neutrino Array) is a surface array of radio receivers that will span 900 km² of the Ross Ice Shelf, and have an effective coverage of half a teraton of ice. Each ARIANNA station contains RF antennas, amplifiers, digitization, real-time triggering, computing power, data storage, local-area networking plus satellite communications, and is powered by both sun and

wind. Two prototype stations have been installed, with an initial seven-station hexagonal array due for deployment over the next two seasons. A photograph of the 2011 station, taken while under construction on the ice, is shown in Fig. 1.

The experiment will detect radio waves originating from high energy neutrino interactions with atoms in the ice via the Askaryan Effect [1]. These interactions generate a shower of secondary particles, and the inelastic scattering of photons and charged particles in this shower give rise to an excess of negatively charged particles, spread over an area of only a few centimeters. Electromagnetic radiation given off by these charged particles is coherent for wavelengths much larger than a few centimeters, resulting in a pulse that is most pronounced for radio wavelengths.

ARIANNA takes advantage of unique geophysical features of the Ross Ice Shelf. The water-ice interface of the ice shelf acts as a nearly perfect mirror for radio pulses generated by extremely high-energy neutrinos traveling downward and interacting in the ice. The ice's long attenuation length allows for the reflected and direct radio pulses to travel to the ice surface where they will be detected by an array of autonomous stations spaced a kilometer apart. The long attenuation length allows for the stations to reside on the surface. This and the ice shelf's relative proximity to McMurdo (120 km away) significantly simplifies the deployment of a large array.

ARIANNA is designed to improve the sensitivity to neutrinos with energies in excess of 10^{17} eV by at least an order of magnitude relative to existing limits [2]. ARIANNA's goals include a confirmation and measurement of the Greisen-Zatsepin-Kuzmin neutrino flux [3], [4], which results from cosmic rays interacting with the diffuse cosmic microwave background. In addition, ARIANNA will be capable of measuring the neutrino cross section at 100 TeV center of mass energy, of searching for point sources of very high energy neutrinos, and it will be sensitive to predicted physics beyond the standard model, such as topological defects produced in the Big Bang. The location of ARIANNA on the Ross Ice Shelf helps provide it with isolation and protection from undesired sources of radio signals, such as man-made sources. A new, sophisticated triggering system will be used to significantly reduce background due to ambient thermal noise, cosmic-ray induced air showers (which produce a different pulse waveform than neutrinos) and intermittent radio pulses from McMurdo.

The U.S. National Science Foundation has approved a three-year R&D funding round for a hexagonal array of ARIANNA stations, to be completed in 2013.

II. WAVEFORM DIGITIZATION INTEGRATED CIRCUIT

The core data acquisition system for the 2011 prototype ARIANNA station consists of 4 signal channels, with each channel

Manuscript received June 15, 2012; revised September 11, 2012; accepted October 23, 2012. Date of current version April 10, 2013. This work was supported by the Office of Polar Programs at the U.S. National Science Foundation (ANT-0839133).

The author is with the University of California, Irvine CA 92697 USA (e-mail: stuartk@uci.edu).

Color versions of one or more of the figures in this paper are available online at <http://ieeexplore.ieee.org>.

Digital Object Identifier 10.1109/TNS.2013.2252365

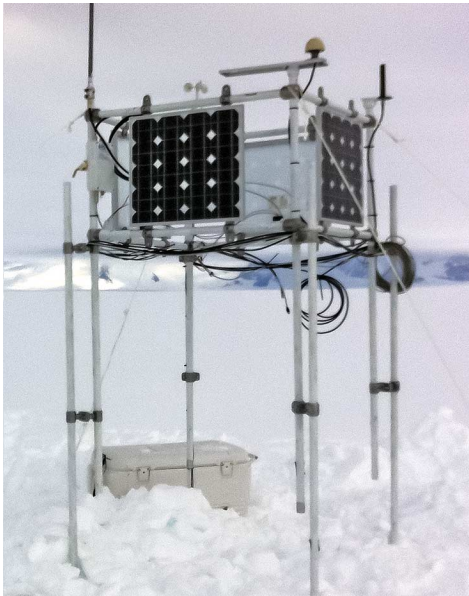


Fig. 1. The 2011 prototype ARIANNA station under deployment. Solar panels, communications (wireless and satellite modem) and GPS antennas are above-surface. Electronics are at/below the surface. Wind power is on a separate mast.

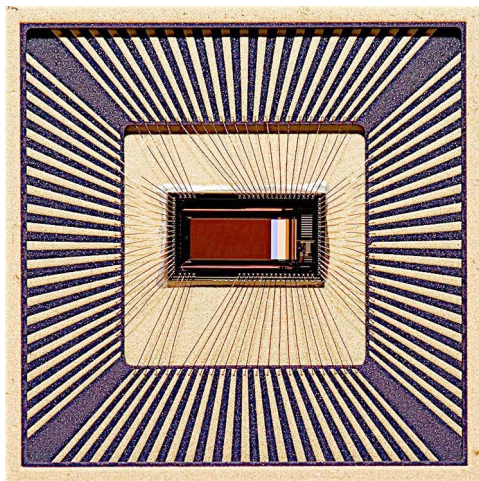


Fig. 2. A die photo of the 2 GHz synchronous ATWD integrated circuit.

performing 2 GHz waveform digitization and real-time triggering via a custom CMOS IC (“Advanced Transient Waveform Digitizer” or ATWD [5]–[8]) and ancillary FPGA logic. A supervisory mother-board containing a 32 bit CPU and flash memory assemblies, stores and transmits the data.

The Advanced Transient Waveform Digitizer chips (Fig. 2) used in the 2011 ARIANNA prototype station are high-speed analog sampling, triggering and digitizing integrated circuits. This new chip [9] continually samples the incoming waveforms at 2 GHz and with over 11 bits of dynamic range. The chip is constructed in a 0.25 micrometer CMOS process. A block diagram of the chip’s internals is shown in Fig. 3.

Unlike previous generations of ATWD’s, this new approach uses synchronous sample clocking, phase-locked to an external reference crystal oscillator, leading to orders of magnitude greater sample timing stability (less than 1 ppm RMS jitter). It also incorporates sophisticated real-time pattern-matching trigger functionality that allows, for example, the detection of

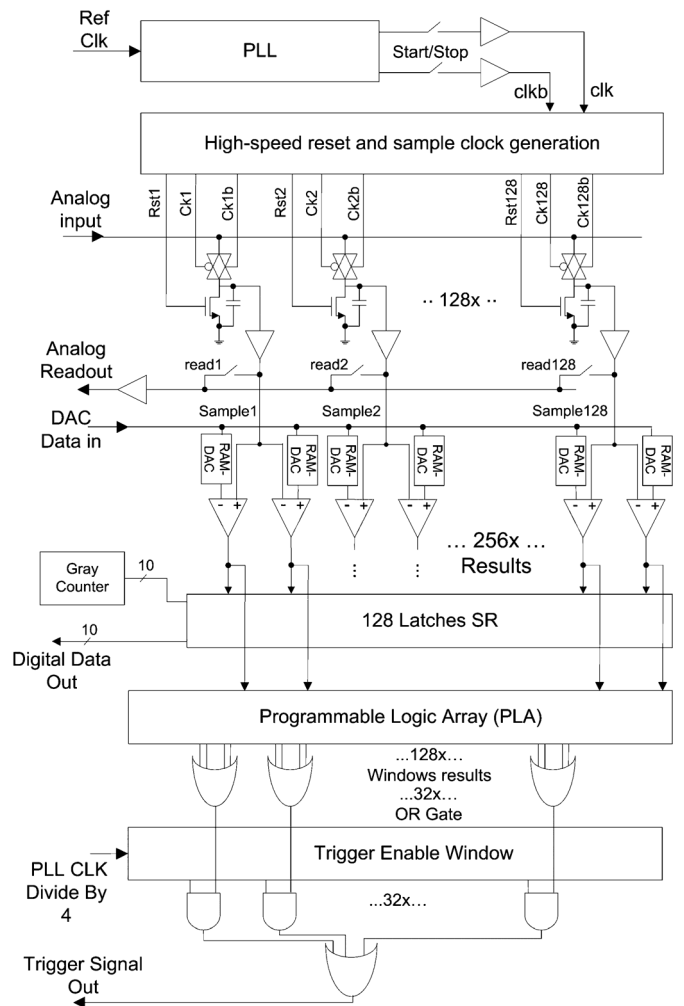


Fig. 3. A block diagram of the 2 GHz synchronous ATWD integrated circuit, showing sampling, comparison, and programmable trigger logic.

a bipolar waveform within a certain magnitude and frequency range. A prompt trigger is produced within about 15 ns of the transient’s arrival, in time for a programmable coincidence between channels to be recognized and the acquisition stopped for readout.

The waveform trigger pattern-matching abilities of the chip are extensive. Up to 72 patterns can be loaded into each chip. Each pattern may be a combination of input signal conditions, namely *H*—the signal must be above a high threshold, *L*—the signal is below a separate low threshold, *N*—neither above nor below (i.e., between the two threshold levels), or *X*—don’t care (does not veto triggers). Each pattern consists of 8 such conditions, representing 8 consecutive samples (see Fig. 4). A trigger pattern of *HXXXLXXX*, for example, looks for a bipolar pulse in which the high and low lobes are about 2 ns apart (at 2 GHz, each sample represents 0.5 ns of time). An additional pattern of *LXXXHXXX* can be added to search for bipolar pulses of either initial polarity. A pattern of *HXNXLXNX* adds specificity in that the waveform must cross at about 1 ns between the high and low lobes, and a pattern of *HHNNLLNN* would be more restrictive still.

The primary goal of pattern matching in the ATWD trigger is to improve selectivity: to allow the use of lower thresholds while suppressing triggers that are merely due to noise, yet still

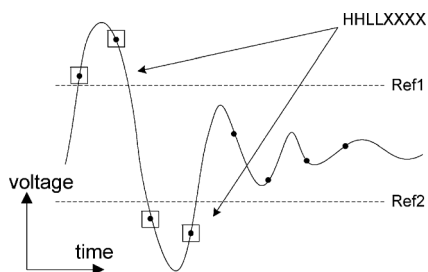


Fig. 4. An example trigger pattern (*HHLXXXX*) searching for two high samples followed by two low samples, followed by four “don’t cares.”

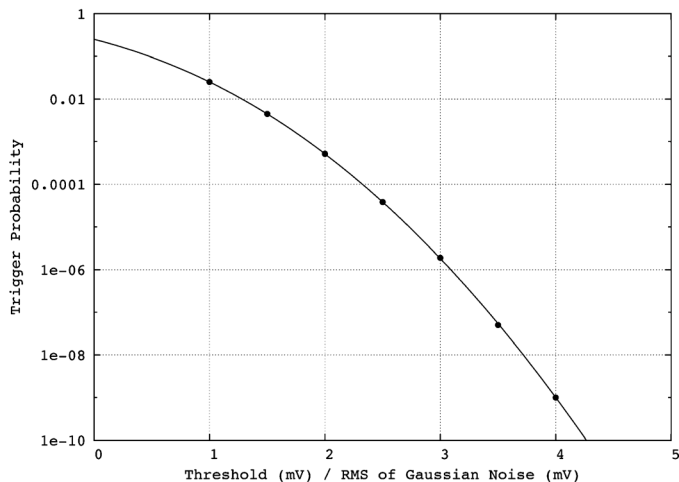


Fig. 5. Probability of triggers due to Gaussian noise versus threshold value. The threshold (X-axis) is shown in proportion to the RMS noise.

capturing a high percentage of signals of genuine interest. As an example of how well pattern matching can help, Fig. 5 shows the probability of triggers due merely to noise as a function of the ratio of the threshold and the RMS noise (Gaussian), given the use of the pattern *HXXLXXXX*. The X-axis shows the analog threshold settings divided by the RMS noise, hence the point at 1 (mV/mV) means that the threshold equals the RMS value of the noise, while 2 means that it is set twice as high as the RMS noise value. It is expected that increasing the threshold reduces the trigger rate. However, using the pattern results in a far more dramatic reduction. By setting the threshold to be three times the RMS noise value (“3 sigma”), for example, the trigger probability drops by nearly 6 orders of magnitude, versus about 3 if a simple single (non-pattern) trigger threshold were used. This simulation was based on one billion white noise events, and sampled by a virtual ATWD at a 1.92 GHz sample rate. In the above 3-sigma case, the trigger rate falls from a rate of order 1 GHz to a rate of order 1 kHz.

Further improvements in noise rejection are achievable if, as implemented, a second-level trigger requiring a coincidence between a combination of closely-spaced ATWD triggers, e.g., “any two triggered channels out of four, coincident within a gate of 20 ns,” is imposed. With the above 3-sigma conditions, and this particular example second-level trigger condition, the above rate of 1 kHz is further reduced to a rate of order 1 Hz. Hence the pattern-matching trigger plus second-level coincidence capability should allow 3–4 sigma thresholds while maintaining a manageable thermal noise trigger rate.

In addition to reducing triggers from noise, the pattern-matching technique must prove able to capture signals of

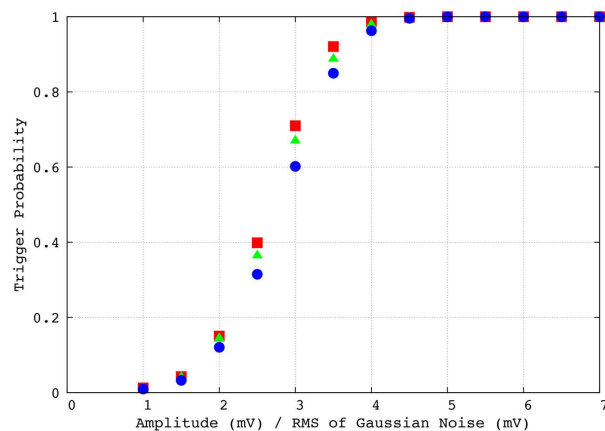


Fig. 6. Probability of triggers on genuine signals versus SNR (x-axis). Points for on-axis antenna signal reception (squares), 45 degrees in the H-plane (triangles) and 90 degrees (circles) are shown.

genuine interest. To simulate this, a genuine ~ 1 ns pulse, driven through a Seavey quad ridge radio horn of 200–1200 MHz bandwidth, and received through an ARIANNA log-periodic dipole array antenna was used as a template for simulations of a signal superimposed on Gaussian noise. In this simulation of 10 000 events, a symmetrical bipolar threshold of 3 sigma (3 times the RMS noise for both high and low thresholds) was imposed. For trigger patterns, every combination of a single *H* and a single *L* was chosen, for 14 patterns in all (i.e., *HLXXXXXX*, *HXLXXXX*, etc., and the inverse *LHXXXXXX*, etc.). This set of patterns is more permissive than a single pattern such as the previous *HXXLXXXX*. Fig. 6 shows the efficiency of triggers resulting from the incoming modeled signal. Here, the X-axis is the amplitude of the signal over the RMS noise (signal to noise ratio). The three sets of points correspond to templates taken at varying angles in the H-plane of the receiver antenna: squares are on-axis, triangles are 45-degrees in the H-plane, and circles are at 90-degrees). The trigger efficiency is seen to be relatively insensitive to the distortion in the time domain caused by the varying angle of incidence. At an SNR of three standard deviations, the trigger pattern is 60–70% efficient, and at four standard deviations it is over 95% efficient at triggering on the genuine incoming signal.

The chip contains a number of other unique features, such as the ability to trim each comparator’s threshold and input offset by the use of per-comparator digital to analog converters (there are 256 comparators per chip, and hence 256 corresponding DAC’s). In addition, the design includes a trigger window system that rejects “stale” triggers that are more than a programmable number of ns old.

As an example waveform, Fig. 7 shows a single, uncorrected, record of samples (dots) from an ATWD chip while acquiring a 20 MHz sine wave. A fitted sine wave is shown superimposed. Random deviations from the fitted waveform are primarily “fixed pattern noise” arising from sample-to-sample variations that are fixed rather than time or signal dependent, and can hence they can easily be subtracted, leaving only about 0.7 mV RMS temporal noise.

III. DATA ACQUISITION SYSTEM

The core ARIANNA prototype DAQ system comprises four channels of ATWD sampling with extensive supporting electronics, and is shown in Fig. 8. Front-end electronics consists of

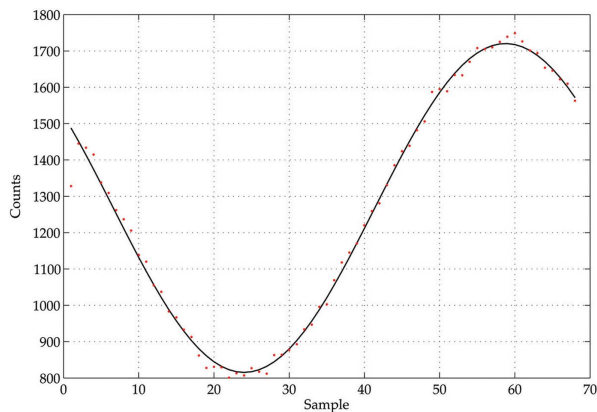


Fig. 7. ATWD readout of an uncorrected sampled 20 MHz sine wave (dots), with a fitted sine wave superimposed (line).



Fig. 8. The core data acquisition system for the 2011 prototype ARIANNA station. Each daughter-card contain an ATWD sampling chip and support circuitry, while the motherboard contains a microcontroller, flash card, and various I/O including USB and trigger inputs and outputs.

four channels of amplification and filtering. Each amplifier includes four AC-coupled 1.5 GHz GaAs gain stages with inter-stage filtering. Additional band-pass filtering was added after the amplifier stages in order to block RF emissions from the communications array, leaving a frequency range of 130–1100 MHz intact. Finally, a limiter circuit was used to prevent very large signal events from saturating the ATWD's.

The ATWD chips continually capture the incoming waveforms at 2 GHz and with over 11 bits of dynamic range. Simultaneous with acquisition, a programmable logic array in each chip searches for patterns in the incoming waveform indicative of signals of interest. For example, for a bipolar impulsive waveform within a certain magnitude and frequency range. Once a board signals a match has been found, logic in the system's FPGA's then look for timing coincidences that indicate that multiple boards have seen the same signal. If a programmed level of coincidence (e.g., three out of four channels) occurs over a preset period of time, a master trigger is delivered and the ATWD's are halted. An on-board 32-bit embedded computer system then supervises the digitization of the ATWD's contents, and saves and transmits the resulting data for further processing.

A main station computer running Linux downloads the data from the acquisition system's embedded CPU, time-stamps it, and stores it on a solid-state hard drive. This system communicates with the outside world by two methods: conventional local-area wireless, including a long-distance directional tower system to McMurdo Station (via a repeater on Mt. Discovery), and satellite modem.

Various configuration parameters are stored on the Linux computer's solid state drive in text format. These parameters can be changed by logging into the CPU remotely and editing the files, or by FTP transfer, etc. The configuration file is used to set trigger system thresholds, the trigger patterns, the number of cards receiving simultaneous triggers required to generate a final trigger, etc. ATWD thermal triggers can be disabled, and/or the time between automatically generated triggers can be set. The latter "forced" trigger initiates data readout without regard for the incoming waveform, and is useful to obtain a collection of data that is free of any bias due to trigger settings. The microcontroller pushes data to the station's CPU, along with a timestamp, a 32-bit CRC of the data and a flag to specify whether the trigger was "thermal" (triggered by the incoming signals) or forced.

Nearly 1.4 million events have been acquired by the second prototype station between December 21, 2011 and March 15, 2012. Each event is packaged by the station's CPU and stored to solid-state flash memory. In addition to all information received from the microcontroller, an event number is assigned, the event is stamped with the CPU's current time in microseconds and a second CRC calculated by the CPU is included. Given the low expected trigger rate, files on disk are managed so as to contain no more than 1000 events in order to minimize the risk of substantial data loss due to file corruption. Files are then pulled off the station remotely using the station's wireless communication systems.

In addition to event data collection, a separate program running on the CPU collects data to monitor the status of the station. This data includes measurements of the current from the various power supply systems, the readout of the station's anemometer and the temperatures on the solar panels as well as inside the station enclosure. These measurements are written to the solid state drive in files that are kept separate from triggered data. A portion of the environmental and status data acquired during the 2011–2012 austral summer is shown in Fig. 9. Extensive power controls are provided so that the station may shut down individual amplifiers, communications modules, etc., in order to conserve power when necessary.

A photo of the 2011 prototype ARIANNA data acquisition system is shown in Fig. 10. Hand-made and partially assembled in the field, it has been almost completely redesigned for the 2012 season, resulting in the much lower-power, lower-cost and far easier to manufacture system discussed in Section V.

Fig. 11 shows an ATWD system's output (solid line) upon receiving a radio signal that was bounced off of the bottom of the ice shelf. Superimposed on this is a comparison with another bounced signal captured via a 1 GHz oscilloscope, which shows similar performance. The -3 dB bandwidth of the ATWD chip meets or exceeds 1 GHz over the signal range of interest, and that of the entire system is at least 700 MHz.

IV. RF ATTENUATION AND REFLECTION MEASUREMENTS

The ARIANNA concept relies on the transparency of ice at radio frequencies and good reflectivity from the ice-water interface at the bottom of the ice shelf. Earlier studies of the ice properties using vertically reflected signals at the ARIANNA site [10]–[12] provided encouraging evidence for field attenuation lengths in excess of 350 m for all relevant frequencies. In those studies, reflective losses were unmeasured, resulting in a default assumption that the reflective losses were small, and the data thus provided a lower bound on the attenuation length. The assumption was justified by the excellent fidelity

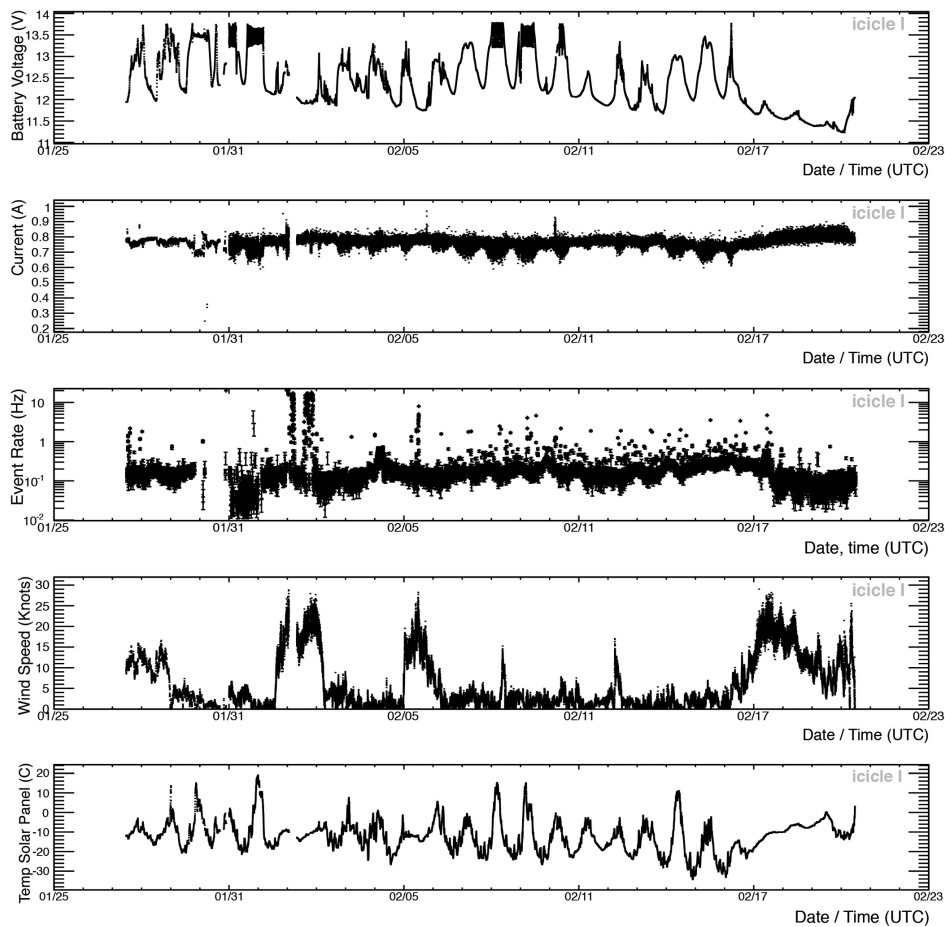


Fig. 9. A portion of the environmental and status data acquired during the 2011–2012 austral summer since installation. From top to bottom, these plots show the battery voltage (V), battery current (Amps, but with arbitrary Y-axis magnitude units), triggered event rate (Hz), wind speed (knots), and outside temperature (C).



Fig. 10. The 2011 prototype ARIANNA station's data acquisition electronics.

of the reflected signal in the time domain, which provided evidence that the reflective surface was flat. With little apparent scattering from the reflective surface and the theoretical expectation that the ice-seawater boundary absorbs less than 4% of the power, it was argued that beam losses due to reflection were small. Studies performed during Antarctic summer campaigns in 2010 and 2011 have measured both the attenuation length and

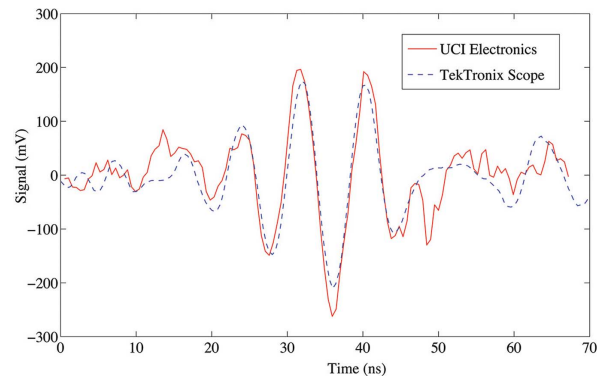


Fig. 11. ATWD output (solid line) upon receiving an RF signal bounced off of the bottom of the Ross Ice Shelf, superimposed on another bounce recorded by a 1 GHz-bandwidth oscilloscope.

reflectivity, and confirmed the earlier assumption of the ice-seawater interface being an excellent reflector of radio power.

In the new studies, a large amplitude, short-duration (about 1 ns FWHM) electrical pulse from a Pockel Cell Driver was transmitted vertically downward and the delayed reflected pulse was observed by a receiver antenna. By comparing the vertically reflected data to similar data collected when the transmitter and receiver were separated horizontally by baselines of 0.5–1 km, it is possible to separate the average losses due to propagation

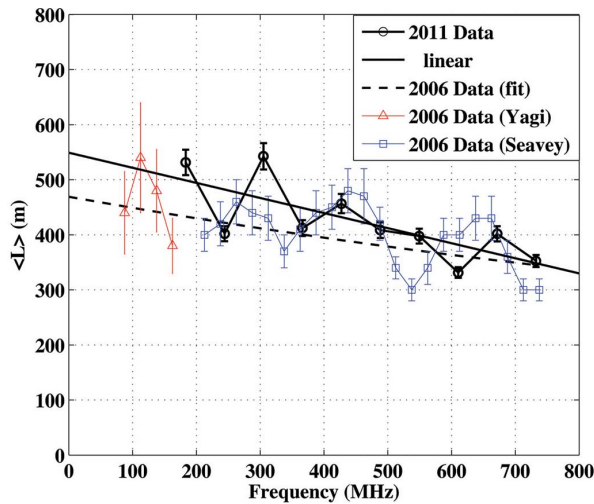


Fig. 12. Preliminary attenuation length $\langle L \rangle$ as a function of frequency (2011 data) and linear fit (solid line) compared to previously published data using two different types of antenna, Yagi and Seavey quad ridge horn.

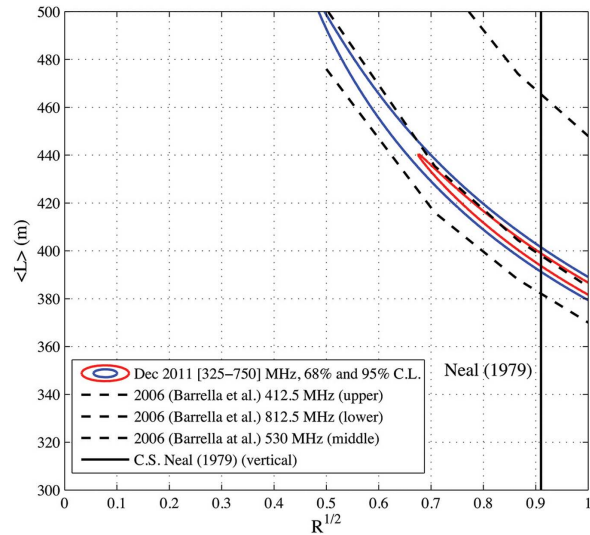


Fig. 13. Contour plots of attenuation length as a function of reflected field shown for 68% confidence limit (inner elongated oval shape), and 95% confidence limit (outer oval) for the frequency interval 325–750 MHz.

and due to reflection. Fig. 12 shows that the most recent, preliminary, results agree with previous measurements of attenuation length at the ARIANNA site (albeit performed at locations that differ by several kilometers). The most recent attenuation-length measurements are systematically larger due to the incorporation of our best estimate of the electric field reflection coefficient, $R^{1/2} = 0.85$.

Measurements shown in Fig. 13, indicate that the electric field reflection coefficient at the ARIANNA site is compatible with theoretical estimates for a flat surface. The two contours show the attenuation length as a function of the reflected field for a 68% confidence limit (inner elongated oval shape), and a 95% confidence limit (outer oval), for the frequency interval 325–750 MHz. The vertical line at 0.91 corresponds to the expected reflection for ideal flat surfaces. The dashed curves compare data to previously published results at specified frequencies within the band.

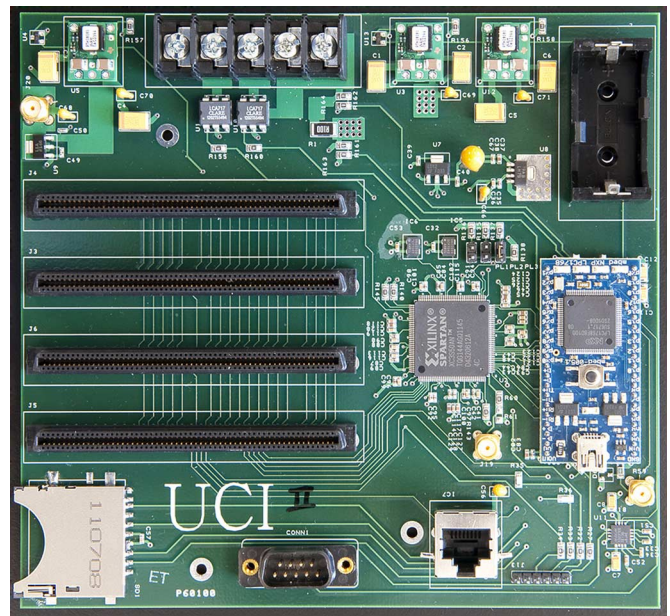


Fig. 14. 2012 ARIANNA station's DAQ mother board. It contains a 32 bit embedded CPU, flash memory for data storage, Ethernet and RS-232 for communications, power control, conditioning and monitoring, fast “heartbeat” pulse generation, real time clock battery backup, an external trigger input, etc.

V. IMPROVED 2012-SEASON DATA ACQUISITION SYSTEM

A new data acquisition system has been prepared for in the 2012–2013 austral summer season. The main advances of this system are substantially reduced power consumption and improved manufacturability, lower cost, improved physical integrity, lighter weight and more compact dimensions.

Improvement in the manufacturability of the station's DAQ system has been very substantial: rather than the hand-made station installed in 2011 and seen in Fig. 10, nearly the entirety of the 2012 DAQ system's functionality has been integrated into easily and inexpensively made printed-circuit boards. Cost savings have been dramatic as well: the new system's motherboard (Fig. 14) costs a small fraction of the components it replaces. A small-scale “mass production” of new systems has been completed as of Spring 2012.

Power consumption has been reduced from ~ 30 W to about 7.5 W in a full power acquisition mode. The factor of four reduction in power maximizes the acquisition time on solar power, and increases the hope of significant winter operation on wind power only. During the summer, when solar power is plentiful, a relatively high-powered wireless link can be maintained with McMurdo bay. When power needs to be conserved, such as during winter, the intermittent use of a low-power Iridium Short Burst Data system allows continued control and monitoring via satellite.

Solar panels perform well in the Antarctic environment due to the high reflectivity of the snow. A large battery is useful for buffering variations in cloud cover, the transition periods between 24-hours of sun or darkness, and the substantial expected pauses in available wind power. Unfortunately, battery capacity and performance metrics such as maximum charging current are much worse than nominally-rated at very cold temperatures. Newer battery technologies such as LiFePo_4 are expected to perform much better than traditional lead-acid batteries, and are being tested and prepared for deployment during the 2012 season.

VI. SUMMARY

A prototype ARIANNA station was installed in late 2011 and ran autonomously during the remainder of the 2011–2012 austral summer. It contains new ATWD sampling chips that operate synchronously with high timing precision, and which deliver real-time triggers based on waveform pattern matching. The station took data via forced periodic triggers and “thermal” triggers. Its data acquisition system includes several means of controlling the rate of such triggers, including DAC-programmable bipolar analog threshold settings, how permissive or restrictive the ATWD’s PLA trigger logic programming is, and the aggressiveness of the coincidence logic (i.e., requiring 2 or 3 or even 4 out of 4 channels to have near-simultaneous triggers). For diagnostic and monitoring purposes, automatic triggers are also generated periodically by the embedded microcontroller or, during tests and installation, by an external trigger much like that used with an oscilloscope. The station records environmental data such as power, temperature and wind velocity. It includes control for the power to major sub-systems and communicates by wireless and satellite modem.

About 1.4 million events were acquired by the second station between December 21, 2011 and March 15, 2012. In addition, measurements in the ice were made by bouncing radio pulses off of the bottom of the ice shelf, demonstrating that the ice-water interface reflects radio waves with very low loss (under 4%), and further confirming the attenuation length in excess of 350 m for all relevant frequencies.

A new, highly-integrated replacement for the hand-made 2011 station was described. It offers a factor of four power reduction, to about 7.5 W, as well as significantly-improved manufacturability and cost.

ACKNOWLEDGMENT

The author wishes to acknowledge support from the Office of Polar Programs at the US National Science Foundation under

Grant ANT-0839133. The author would also like to thank W. Huang and S. Wood Chiang for their effort designing the ATWD circuit, and J. Hinderlie, N. Rott, and B. Sass for their assistance with the installation of the prototype ARIANNA station.

REFERENCES

- [1] G. A. Askaryan, *JETP*, vol. 14, p. 441, 1962.
- [2] K. Dookayka, “Characterizing the Search for Ultra-High Energy Neutrinos with the ARIANNA Detector,” Ph.D. dissertation, Univ. of CA, Irvine, USA, 2011.
- [3] K. Greisen, “End to the cosmic-ray spectrum?,” *Phys. Rev. Lett.*, vol. 16, no. 17, pp. 748–750, 1966.
- [4] G. T. Zatsepin and V. A. Kuz’min, “Upper limit of the spectrum of cosmic rays,” *J. Experimental Theoretical Phys. Lett.*, vol. 4, pp. 78–80, 1966.
- [5] S. A. Kleinfelder, “A Multi-Gigahertz Analog Transient Waveform Recorder Integrated Circuit,” Masters thesis, Univ. of CA, Berkeley, 1992.
- [6] S. A. Kleinfelder, “Advanced transient waveform digitizers,” in *Proc. SPIE Particle Astrophys. Instrumentation*, Aug. 2002, vol. 4858, pp. 316–326.
- [7] S. A. Kleinfelder, “A multi-GHz, multi-channel transient waveform digitization integrated circuit,” in *Proc. IEEE Nucl. Sci. Symp.*, Orlando, FL, Oct. 2002.
- [8] S. A. Kleinfelder, “GHz waveform sampling and digitization circuit design and implementation,” *IEEE Trans. Nucl. Sci.*, vol. 50, no. 4, pp. 955–962, Aug. 2003.
- [9] W. Huang, S. W. Chiang, and S. Kleinfelder, “Waveform digitization with programmable windowed real-time trigger capability,” in *Proc. IEEE Nucl. Sci. Symp.*, Orlando, FL, Oct. 2009.
- [10] C. S. Neal, “The dynamics of the Ross Ice Shelf revealed by radio echo-sounding,” *J. Glaciology*, vol. 24, pp. 295–307, 1979.
- [11] T. Barrella, S. Barwick, and D. Saltzberg, “Ross Ice Shelf in situ radio-frequency ice attenuation,” Nov. 1, 2010, arXiv.org. Doi:10.3189/002214311795306691.
- [12] J. Hanson, “Ross Ice Shelf thickness, radio-frequency attenuation and reflectivity: Implications for the ARIANNA UHE neutrino detector,” in *Proc. 2011 Int. Cosmic Ray Conf.*, Beijing, China, for the ARIANNA Collaboration.